Magneto−Optical Investigation of the Exchange-Coupled Dimer $Cs_3Mo_2Br_9$

Robert Stranger,*,† Lucjan Dubicki,*,‡ and Elmars Krausz‡

Department of Chemistry and Research School of Chemistry, The Australian National University, Canberra, ACT 0200, Australia

Received December 13, 1995⊗

The electronic spectrum of the confacial bioctahedral complex $Cs_3Mo_2Br_9$ has been investigated by single-crystal absorption, Zeeman, and MCD spectroscopies. A total of seven distinct band regions were resolved and assigned to transitions essentially within the $t_2^2t_2^2$ configuration that arises when the pair of t_{2z} orbitals in the $t_2^3t_2^3$ configuration is decoupled by strong Mo−Mo σ bonding. The excited state separations, and in particular the orbital g values, are sensitive to Mo−Mo π bonding and show clearly that the π bonding is weaker in the bromide than in the chloride complex.

Introduction

$Cs_3Mo_2Br_9$ is a member of the classic series of face-shared bioctahedral dimer complexes $A_3M_2X_9$ where the structural, magnetic, and spectroscopic properties are strongly influenced by the nature of the metal ion M^{3+}, halide X, and univalent cation A.[1−8] Even within the series $Mo_2X_9^{3-}$ (X = Cl, Br, I), significant structural differences exist.[6,7] For instance, the Mo−Mo bond distance of 2.65 Å in $Cs_3Mo_2Cl_9$ increases to 2.82 Å in $Cs_3Mo_2Br_9$. These structural changes are reflected in the observed magnetic properties with the ground state singlet−triplet splitting decreasing from 840 cm^{-1} for the chloride to 760 cm^{-1} for the bromide complex.[8] The variation in magnetic properties can be largely attributed to a decrease in Mo−Mo bonding with increasing Mo−Mo separation, as shown in a recent Xα−SW study of the $A_3Mo_2X_9$ (X = Cl, Br, I) system.[9]

A magneto−optical study[10,11] of $Cs_3Mo_2Cl_9$ showed that the absorption bands below 17 000 cm^{-1} could not be understood with a simple molecular-orbital model. Configuration interaction is very large, and the multiplet splittings should be better described by the exchange-coupled-pair model. The application of the pair model to the $t_2^3t_2^3$ configuration showed that as the Mo−Mo σ bonding between the t_{2z} orbitals becomes very large, the lowest set of multiplets converged to those derived from the $t_{2e}^2t_{2e}^2$ configuration where t_{2e} are the t_{2x} and t_{2y} orbitals which are involved in Mo−Mo π and δ bonding. Thus, for $Cs_3Mo_2Cl_9$, the exceptionally low energy of the sharp lines near 7800 cm^{-1} could be explained as a consequence of the lower interelectronic repulsion energy, $6B + 2C$, between the multiplets $^3A_2{}^3A_2$ and $^3A_2{}^1E$ compared to $9B + 3C$ for the $^4A_2{}^4A_2$ and $^4A_2{}^2E$ multiplets that maintain their identity in the regime of small Mo−Mo σ bonding. Furthermore, the observation of sharp lines near 13 000 cm^{-1} that had no MCD could be simply explained by assigning the lines to double excitations within the $t_{2e}^2t_{2e}^2$ configuration.

The strong Mo−Mo σ bonding was firmly established, but the magnitude of J_π (see Theory) was uncertain for several reasons. Only one spin−orbit level (E′) of the first excited state $^3E''(A_1' + A_2' + E' + E'')$ was detected. The orbital g value for the $^3E''(E')$ level was found to be, surprisingly and inexplicably, very small, $k \sim 0.3$. Further, we assumed that the same k could be transferred to other multiplets. This led to difficulties in identifying the second excited state $^3E'$ and to an incorrect assignment of the doubly excited $|(^1E^1E)^1E'\rangle$ state.

The extension of the pair model to include e_g orbitals[12] provided a possible solution to the orbital g value problem[13] as well as providing a theoretical basis for the analysis of the broad spin-allowed bands above 17 000 cm^{-1}.[14] In addition, a study of the splitting of the $|(^1E^1E)^1A_1', {}^1A_1''\rangle$ levels[11] provided more evidence for the growing belief that Mo−Mo π bonding was moderately large.

With the availability of superior detectors, we have reexamined the spectra of $Cs_3Mo_2X_9$ (X = Cl, Br) in order to obtain more accurate g values, resolve some of the band assignments, and determine the extent of Mo−Mo π bonding. This paper deals with the magneto−optical study of $Cs_3Mo_2Br_9$ and a comparison with $Cs_3Mo_2Cl_9$.

Experimental Section

Preparation of Crystals. Crystals of $Cs_3Mo_2Br_9$ were grown by slow vapor deposition. The procedure was similar to that used in preparing crystals of $Cs_3Mo_2Cl_9$.[10] The chloride crystals exhibited some strain under cross-polarizers. The bromide crystals were strain-free, and this was confirmed by resolving and proving that the $^1A_1' \rightarrow {}^3E''(E'')$ transition was pure magnetic dipole allowed (see Band 1 section).

Crystal Structures. $Cs_3Mo_2Br_9$ crystallizes in the space group D_{6h}^4−$P6_3/mmc$ with $Z = 2$ and is isomorphous with $Cs_3M_2X_9$, where M = Cr, Mo, and W and X = Cl, Br, and I.[5−7] The bond distances for Mo−Mo, Mo−Br(bridge), and Mo−Br(terminal) are 2.82, 2.62, and 2.54 Å, respectively. The cone angle (angle between the Mo−Br bond

---

* Authors to whom correspondence should be addressed.

† Department of Chemistry.

‡ Research School of Chemistry.

⊗ Abstract published in *Advance ACS Abstracts,* June 1, 1996.

(1) Grey, I. E.; Smith, P. W. *Aust. J. Chem.* **1969**, *22*, 121.
(2) Dubicki, L.; Ferguson, J.; Harrowfield, B. V. *Mol. Phys.* **1977**, *34*, 1545.
(3) Briat, B.; Kahn, O.; Morgenstern-Badarau, I.; Rivoal, J. C. *Inorg. Chem.* **1981**, *20*, 4193.
(4) Leuenberger, B.; Briat, B.; Canit, J. C.; Furrer, A.; Fischer, P.; Güdel, H. U. *Inorg. Chem.* **1986**, *25*, 2930.
(5) Watson, W. H.; Waser, J. *Acta Crystallogr.* **1958**, *11*, 689.
(6) Saillant, R.; Jackson, R. B.; Streib, W. E.; Folting, K.; Wentworth, R. A. D. *Inorg. Chem.* **1971**, *10*, 1453.
(7) Stranger, R.; Grey, I. E.; Madsen, I. C.; Smith, P. W. *J. Solid State Chem.* **1987**, *69*, 162.
(8) Stranger, R.; Smith, P. W.; Grey, I. E. *Inorg. Chem.* **1989**, *28*, 1271.
(9) Medley, G. A.; Stranger, R. *Inorg. Chem.* **1994**, *33*, 3976.
(10) Dubicki, L.; Krausz, E.; Stranger, R.; Smith, P. W.; Tanabe, Y. *Inorg. Chem.* **1987**, *26*, 2247.
(11) Stranger, R. *Chem. Phys. Lett.* **1989**, *157*, 472.
(12) Stranger, R. *Inorg. Chem.* **1990**, *29*, 5231.
(13) Stranger, R.; Moran, G.; Krausz, E.; Dubicki, L.; Güdel, H.; Furer, N. *Inorg. Chem.* **1992**, *31*, 2860.
(14) Stranger, R.; Moran, G.; Krausz, E.; Medley, G. *Inorg. Chem.* **1993**, *32*, 4555.

S0020-1669(95)01581-3 CCC: $12.00

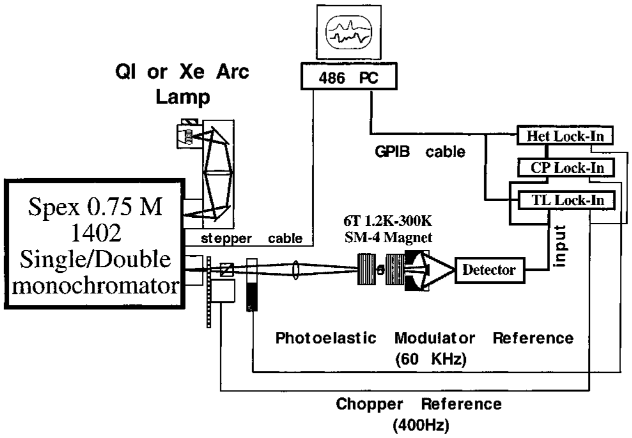

Figure 1. Schematic diagram of the absorption and MCD equipment.

and the molecular trigonal *Z* axis) for the terminal bromide ligands is 55.3°, close to the octahedral value of 54.7°. The cone angle for the bridging bromide ligands is significantly larger, 57.5°, indicating a compression along the *Z* direction caused by the Mo−Mo bonding.

MCD and Absorption Equipment. A schematic figure of our spectrometer is presented in Figure 1. The system was built around a Spex 1402 which operated as either a single or double (0.75 m) monochromator. A damped high-speed stepper motor was fitted to the original unit, which allowed precise wavelength movements, quickly and reproducibly under control of the PC. The gratings used were a 1200 line/mm grating blazed at 500 nm and 600 line/mm gratings blazed at 1 and 1.6 μm. The light source was usually a 24 V, 250 W quartz halogen lamp, imaged 1:1 on the entrance slit. The lamp was run in a cooled housing through a stabilized power supply.

The available range of detectors contributed significantly to the performance of this system and the quality of the data. We used a Hamamatsu R-269 (S-5) tube in the 300−700 nm range and a R-669 (extended S-20) tube in the 400−850 nm range. These tubes were of semitransparent design and gave optimal stability and baseline performance. For high-resolution measurements in the 700−900 nm region a Hamamatsu 943-02 Cs/GaAs photomultiplier was utilized. A liquid-nitrogen-cooled, low-capacitance, 1 mm diameter InSb diode (Cincinatti) was used with an optimized transimpedance amplifier unit in the range from 850 to 1700 nm together with custom reflecting condensing optics.

The system featured three lock-in amplifiers in a heterodyning arrangement. Light was chopped at 400 Hz and the polarization modulated at 60 kHz. A Princeton Applied Research 124A lock-in amplifier (marked CP in Figure 1) measured the signal at 60 kHz. Its output, when operated at maximum bandwidth, was sent to one (marked Het) of the two Stanford Research SR510 lock-in amplifiers, both referenced to the 400 Hz chopper frequency. The Het lock-in provided the signal that was modulated at both 400 Hz and 60 kHz and consequently strongly rejected the interference from either the modulator or the chopper. The detector output was also fed to the second SR510 (marked TL) which measured the total light level.

The 486 PC was fitted with a National Instruments GPIB-PC2A interface card and Metrobyte Mstep-5 stepper motor driver card. The former allowed the PC to fully control the SR510 lock-in amplifiers. The latter provided ramped stepper motor drive pulse trains to move the wavelength of the monochromator. An important feature of this arrangement was that the gain of the two SR510's was automatically adjusted. This provided the necessary wide dynamic range for accurate measurement of MCD and absorption over an extended wavelength range. This system was an extension of the approach used in our versatile single-beam-polarized single-crystal spectrometer.[15] The PC calculated the ratios of the output of the Het and TL lock-in amplifiers to give both the MCD and absorption.

The magneto−optical cryostat was a 6T SM-4 Oxford Instruments Spectromag unit.

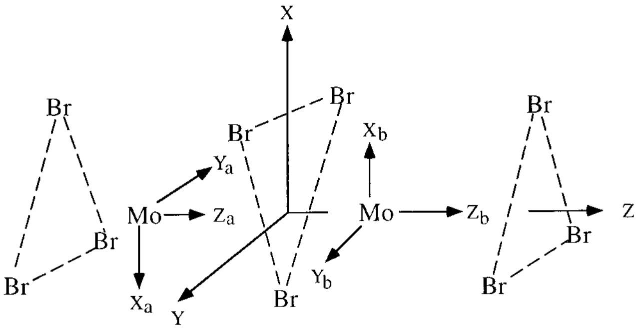

Figure 2. Schematic drawing of the $[Mo_2Br_9]^{3-}$ ion with D_{3h} symmetry. The d orbitals of each Mo(III) ion are defined with respect to the trigonal axes (X_a, Y_a, Z_a) and (X_b, Y_b, Z_b) on centers *a* and *b*, respectively (see text).

Theory

Exchange-Coupled-Pair Model. The exchange Hamiltonian and the coordinate system have been described elsewhere.[10,12] We summarize here the details relevant to this paper. In the exchange-coupled-pair model, strong metal−metal bonding or strong superexchange across bridging ligands is represented by large transfer integrals in the kinetic exchange terms. Within the kinetic exchange approximation, all terms in the exchange Hamiltonian are neglected except those that contain the transfer integrals. In this approximation the exchange Hamiltonian can be written as

$$H_{ex} = {}^1\!/_2 \sum_{\substack{a(\alpha\alpha') \\ b(\beta\beta')}} J(\alpha\alpha',\beta\beta')[-n_a(\alpha\alpha')\, n_b(\beta\beta') - 4S_a(\alpha\alpha')\cdot S_b(\beta\beta') + \delta(\beta\beta')\, n_a(\alpha\alpha') + \delta(\alpha\alpha')\, n_b(\beta\beta')] \quad (1)$$

where the orthogonalized d orbitals α and β belong to metal ions on centers *a* and *b*, respectively, and the sum is over all d orbitals. The generalized occupation numbers $n(\alpha\alpha')$ and spin operators $S(\alpha\alpha')$ which apply to orbital changes as well as spin-flips have been defined earlier.[12] In the kinetic approximation

$$-2J(\alpha\alpha',\beta\beta') = 4h(\alpha,\beta')\, h(\beta,\alpha')/U \quad (2)$$

where $h(\alpha,\beta)$ is the transfer integral between orthogonalized α and β metal d orbitals on centers *a* and *b*, respectively, and *U* is the usual transfer energy. For cases where $\alpha = \alpha'$ and $\beta = \beta'$, we use the simplified notation $J(\alpha\alpha,\beta\beta) = J(\alpha,\beta)$.

Figure 2 gives a schematic drawing of the structure of the $[Mo_2Br_9]^{3-}$ ion. The choice of coordinate axes is the same as in our earlier work.[2,10] The spin functions and all operators are defined with respect to the matched set of trigonal axes, the single-ion (X_a', Y_a', Z_a') and (X_b, Y_b, Z_b) and the pair (*X*, *Y*, *Z*) axes where $X_a' = -X_a$, $Y_a' = -Y_a$, and $Z_a' = Z_a$. The orbital functions on the Mo ions are defined with respect to (X_a, Y_a, Z_a) and (X_b, Y_b, Z_b) axes, respectively, so that the same transformation connects the cubic and trigonal basis on each center. Thus, for both centers *a* and *b*, the real trigonal orbitals which diagonalize the cubic field, denoted by the simplified notation (t_{2x}, t_{2y}, t_{2z}) or (*x*, *y*, *z*), are related to the real cubic orbitals[16] through

$$t_{2x} = (2\zeta - \xi - \eta)/\sqrt{6}$$

$$t_{2y} = (\xi - \eta)/\sqrt{2}$$

$$t_{2z} = (\xi + \eta + \zeta)/\sqrt{3}$$

$$e_x = e_u$$

$$e_y = e_v \quad (3)$$

The t_{2z} orbitals are optimized for Mo−Mo σ bonding in the D_{3h} Cs$_3$-

---

(15) Krausz, E. *Aust. J. Chem.* **1993**, *46*, 1041.

(16) Sugano, S.; Tanabe, Y.; Kamimura, H. *Multiplets of Transition Metal Ions in Crystals*; Academic Press: New York, 1970.

(17) Hopkins, M. D.; Gray, H. B.; Miskowski, V. M. *Polyhedra* **1987**, *6*, 705.

(18) Krausz, E.; Stranger, R.; Dubicki, L. Unpublished data.

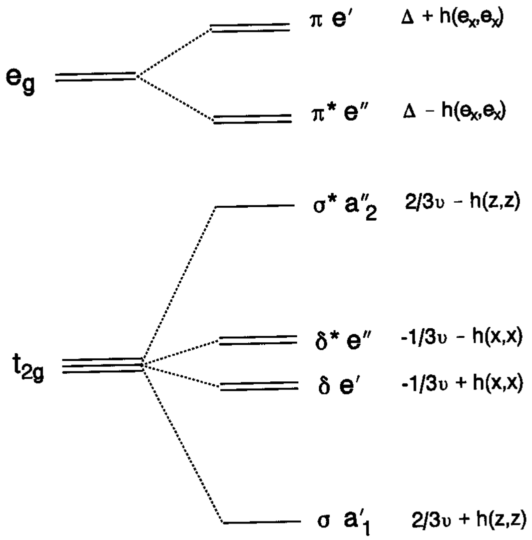

Figure 3. Molecular orbitals for $Cs_3Mo_2Br_9$ and the correspondence of their energies with the single-ion ligand field parameters Δ, υ, and transfer integrals $h(\alpha,\beta)$ (see text).

Mo_2X_9 dimer. They form the σ and σ^* molecular orbitals of a_1' and a_2'' symmetries, respectively, with the energy separation

$$E(\sigma) - E(\sigma^*) = 2h(z,z) \qquad (4)$$

The t_{2x} and t_{2y} orbitals are collectively labeled as t_{2e} and form nominally $^1/_3\pi$ and $^2/_3\delta$ Mo−Mo bonds. The corresponding molecular orbitals are $\delta e'$ and $\delta^* e''$, with the energy separation

$$\begin{aligned} E(\delta) - E(\delta^*) &= 2h(x,x) \\ &= 2h(y,y) \end{aligned} \qquad (5)$$

Similarly, the e_x and e_y orbitals form nominally $^2/_3\pi$ and $^1/_3\delta$ Mo−Mo bonds and the corresponding molecular orbitals are $\pi e'$ and $\pi^* e''$. In this case, superexchange through the σ-bonding framework of the bridging ligands is more important than Mo−Mo bonding and reverses the sign of the transfer integral so that

$$E(\pi) - E(\pi^*) = 2h(e_x,e_x) \qquad (6)$$

is a positive quantity.[9]

The exchange parameter in (1) that describes the Mo−Mo σ bonding is

$$\begin{aligned} -2J(z,z) &= 4h(z,z)^2/U \\ &= J_\sigma \end{aligned} \qquad (7)$$

where we use the simplified notation $J(zz,zz) = J(z,z)$. The corresponding parameter for the t_{2e} orbitals is

$$-2J(x,x) = 4h(x,x)^2/U \qquad (8)$$

In the earlier work[10] we wished to compare the exchange interactions between a standard Mo−Mo σ and a standard Mo−Mo π bond and accordingly introduced the parameter

$$\begin{aligned} J_\pi &= 9 \times 4h(x,x)^2/U \\ &= 9 \times (-2J(x,x)) \end{aligned} \qquad (9)$$

The parameter J_π is used again in this paper although its utility is somewhat spoiled by the fact that $h(x,x)$ contains not only the negative contribution from Mo−Mo π bonding but also a positive contribution from π bonding between the metal and bridging ligand orbitals.

Figure 3 shows the ordering of the molecular orbitals for $Cs_3Mo_2Br_9$ obtained from a spin-restricted Xα−SW calculation.[9] The molecular orbital energies can be expressed in terms of the single-ion ligand field parameters and the transfer integrals of an effective one-electron Hamiltonian, as in the angular overlap model.[19] The diagonal matrix elements in Figure 3 should be supplemented by two off-diagonal elements, $\langle\pi|H_{\mathrm{eff}}|\delta\rangle = \upsilon' + h(e_x,x)$ and $\langle\pi^*|H_{\mathrm{eff}}|\delta^*\rangle = \upsilon' - h(e_x,x)$. Δ is the cubic ligand field, υ and υ' are the standard trigonal field parameters,[16] and the molecular orbital splittings are simply twice the transfer or resonance integral.

Table 1. Ordering of the Low-Energy Multiplets of $[Mo_2Br_9]^{3-}$ in the Limit of Strong σ Mo−Mo Bonding, Zero π Mo−Mo Bonding, and Zero Spin−Orbit Coupling

$(t_{2e})^2(t_{2e})^2$ multiplet	D_{3h} states	interelectronic repulsion energy[a]
$^1A_1{}^1A_1$	$^1A_1'$	$24B$
$^1E^1A_1$	$^1E',^1E''$	$18B + 6C$
$^1E^1E$	$^1A_1'',^1A_1',^1E'$	$12B + 4C$
$^3A_2{}^1A_1$	$^3A_1'',^3A_2'$	$12B + 4C$
$^3A_2{}^1E$	$^3E'',^3E'$	$6B + 2C$
$^3A_2{}^3A_2$	$^1A_1',^3A_2'',^5A_1'$	0

[a] B and C are the Racah interelectronic repulsion parameters.

In the exchange-coupled-pair calculations to follow, we have ignored the trigonal field parameters υ and υ'. The Xα−SW calculations suggest that υ is approximately 0 and -450 cm^{-1} for the bromide and chloride complexes, respectively. The off-diagonal trigonal field parameter, υ', can be nonvanishing because of the trigonal compression of the bridging Mo−X σ bonds. Estimates based on the angular overlap model[19] indicate that υ' is less than 1000 cm^{-1} and is of positive sign. The mixing of e_g and t_{2g} orbitals in $Cs_3Mo_2X_9$ (X = Cl, Br) is therefore expected to be dominated by a pair mechanism involving $h(x,e_x)$ (eq 10).

Since the σ Mo−Mo bonding is strong, the ground configuration for $Cs_3Mo_2Br_9$ is $\sigma^2(\delta\delta^*)^4$. The molecular orbital model does not give a simple description of the lower lying electronic states. The latter can be obtained only after calculating the configuration interaction between the states originating from $\delta^1\delta^{*3}$ and $\delta^3\delta^{*1}$ configurations (Γ' states) and from δ^4, δ^{*4}, and $\delta^2\delta^{*2}$ configurations (Γ'' states).

The interelectronic repulsion energies of the d electrons are relatively large, and a simple description is obtained if we use an exchange-coupled-pair model. Provided the Mo−Mo σ bonding is strong, the t_{2z} orbitals can be decoupled and the lower lying states will be derived from the $(t_{2e}e)^2(t_{2e}e)^2$ configuration. The single-ion $(t_{2e})^2$ configuration in C_{3v} site symmetry gives $^3A_2$, ^1E, and $^1A_1$ states with relative energies 0, $6B + 2C$, and $12B + 4C$, where B and C are the Racah interelectronic repulsion parameters. Table 1 lists all the multiplets derived from the $(t_{2e})^2(t_{2e})^2$ configuration in order of increasing interelectronic repulsion energy. As noted earlier[10] and emphasized in the Introduction, this model is a good starting point for assigning the main features of the optical spectra given in Figures 7 and 8.

The spin-restricted Xα−SW calculations[9] give the following estimates for the transfer integrals, $h(z,z) = -10\,400$ (-7800) cm^{-1}, $h(x,x) = -2000$ (-1100) cm^{-1}, and $h(e_x,e_x) = 1400$ (1900) cm^{-1} for $Cs_3Mo_2X_9$ where X = Cl (Br). By using eqs 7 and 9 we obtain $J_\pi \sim J_\sigma/3$ and $J_\pi \sim J_\sigma/6$ for the chloride and bromide complexes, respectively. Since J_σ must be very large ($\geq 15\,000$ cm^{-1}),[10] it is clear that J_π is also moderately large.

The first attempt at calculating the low-lying excited states of $Cs_3Mo_2Cl_9$ applied the pair model to the $t_2{}^3t_2{}^3$ configuration.[10] Inspection of Figures 11 and 12 in ref 10 shows that, for $J_\pi \sim J_\sigma$ and $J_\sigma \sim 15\,000$ cm^{-1}, the calculated ordering of the excited states is similar to that obtained empirically in this paper.

The above model could not account for the low orbital g values observed in the first excited state of the chloride complex. If J_π is indeed large, then the neglect of e_g orbitals is not valid because Mo−Mo π bonding will mix e_g and t_{2g} orbitals through the nonvanishing $h(x,e_x)$. If both the small δ Mo−Mo bonding and the contribution from the bridging ligands are ignored, then one can derive

$$h(x,e_x) = -\sqrt{2}h(x,x) \qquad (10)$$

The inclusion of e_g orbitals into the d^3d^3 basis makes the pair problem

---

(19) Schäffer, C. E. *Pure Appl. Chem.* **1970**, *24*, 361.

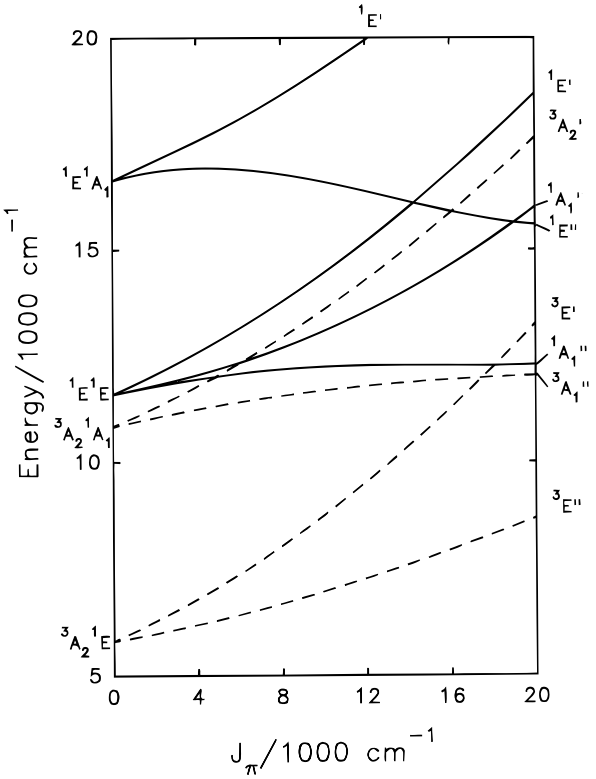

Figure 4. Calculated energy levels for the lower lying excited states of the $(t_{2e}{}^{2-n}e^n)_a(t_{2e}{}^{2-n}e^n)_b$ configurations as a function of metal−metal π interaction J_π. The levels are plotted relative to the ground state at zero energy. The Racah interelectronic parameters are $B = 400$ cm^{-1}, $C = 4B$, the cubic field parameter $\Delta = 20\,000$ cm^{-1}, the transfer integrals $h(e_x,e_x) = 2000$ cm^{-1}, and $h(x,e_x) = -\sqrt{2}h(x,x)$, as in eq 10, and the transfer energy $U = 20\,000$ cm^{-1}. Dashed and full lines correspond to the $S = 1$ and $S = 0$ pair levels, respectively. The pair states are labeled by the $t_{2e}{}^2t_{2e}{}^2$ parentage on the left and by the representation of the molecular D_{3h} point group on the right.

very complicated. As a first approximation, advantage is taken of the strong Mo−Mo σ bonding to restrict the basis to $(t_{2e}{}^{2-n}e^n)_a(t_{2e}{}^{2-m}e^m)_b$ where m and n take the values 0, 1, and 2. The details of this model, labeled hereafter as $(t_{2e}e)^2(t_{2e}e)^2$ have been given[12] and the calculated energy levels for $Cs_3Mo_2Br_9$ are given in Figure 4.

In this model the t_{2z} orbitals are assumed to be completely decoupled by the strong σ Mo−Mo bond. The limitations of this assumption, and the consequent neglect of cross-exchange terms $J_{\sigma\pi}$, may lead to some error in the value of J_π, which is treated as an adjustable parameter. The effect of the e_g−t_{2g} mixing on the orbital reduction parameters has been investigated.[12] This previous work employed the assumption that $h(e_x,e_x) = 2h(x,x)$ which is valid only for pure Mo−Mo bonding. These calculations were repeated with the more realistic values for $h(e_x,e_x)$ obtained from the Xα−SW calculations; *viz.*, $h(e_x,e_x) = 2000$, and $h(x,x)$, which has a negative sign, was varied. This refinement did not alter the dependence of the reduction parameters on J_π except to cause a small change in the magnitudes (next section).

Magnetic *g* Factors. The g values are listed in Table 2 and require some comment. We have neglected spin−orbit coupling in the pair calculations simply because at the level of the $(t_{2e}e)^2(t_{2e}e)^2$ model the spin−orbit matrices are extremely large. In most cases such an omission would be unjustified and lead to meaningless g values. However, in $Cs_3Mo_2X_9$ (X = Cl, Br) the large energy separations between the observed multiplets (see Figures 6 and 7) that are caused by interelectronic repulsion and π Mo−Mo bonding will tend to quench the effects of spin−orbit coupling so that spin should be a fairly good quantum number. Consider the first excited multiplet $^3E''$. The wave functions for the spin−orbit components can be written as $|(S\Gamma)t\tau\rangle = |SM_S\Gamma M\rangle$

$$|(^3E'')E_\pm{}''\rangle = |\pm1\ E_\pm{}''\rangle$$

$$|(^3E'')E_\pm{}'\rangle = |0\ E_\pm{}''\rangle$$

$$|(^3E'')A_1{}',A_2{}'\rangle = |\mp1\ E_\pm{}''\rangle \tag{11}$$

Table 2. Lowest Energy States for $Cs_3Mo_2X_9$ (X = Cl, Br)

$t_{2e}{}^2t_{2e}{}^2$ parentage $\lvert\pm S_a\Gamma_aS_b{}'\Gamma_b{}'S\Gamma\rangle$[a]	D_{3h} spin−orbit level	band assignt[b]	transition dipole[c]	Zeeman term ($B\|z$)[d]
$\lvert^3A_2{}^3A_2{}^1A_1{}'\rangle$	$A_1{}'$			
$\lvert-{}^3A_2{}^1E^3E''\rangle$	$E_\pm{}''$	b1	$m_{x,y}$	$\pm2k_e$
	$A_1{}' + A_2{}'$		m_z	$\mp(g - 2k_e)$
	$E_\pm{}'$		$p_{x,y}$	$\mp(g + 2k_e)$
$\lvert+{}^3A_2{}^1E^3E'\rangle$	$A_1{}'' + A_2{}''$	b2	p_z	$\mp(g - 2k_e)$
	$E_\pm{}'$		$p_{x,y}$	$\pm2k_e$
	$E_\pm{}''$		$m_{x,y}$	$\mp(g + 2k_e)$
$\lvert-{}^3A_2{}^1A_1{}^3A_1{}''\rangle$	$A_2{}''$	(b2)	p_z	
	$E_\pm{}'$		$p_{x,y}$	$\pm g$
$\lvert-{}^1E^1E\ {}^1A_1{}''\rangle$	$A_1{}''$	b3		
$\lvert+{}^1E^1E\ {}^1A_1{}'\rangle$	$A_1{}'$	b4		
$\lvert+{}^3A_2{}^1A_1{}^3A_2{}'\rangle$	$A_1{}'$	b5		
	$E_\pm{}''$		$m_{x,y}$	$\pm g$
$\lvert-{}^1E^1A_1{}^1E''\rangle$	$E_\pm{}''$	b6	$m_{x,y}$	$\pm2k_e$
$\lvert^1E^1E^1E'\rangle$	$E_\pm{}'$	b7	$p_{x,y}$	$\mp4k_e$

[a] $|\pm(S_a\Gamma_aS_b{}'\Gamma_b{}')S\Gamma\rangle = (1/\sqrt{2})[|(S_a\Gamma_aS_b{}'\Gamma_b{}')S\Gamma\rangle \pm |(S_a{}'\Gamma_a{}'S_b\Gamma_b)S\Gamma\rangle]$. [b] The band assignments follow Figures 6 and 7. See text. [c] The magnetic dipole (m_α) and electric dipole (p_α) allowed transitions from the ground state $^1A_1{}'$ appear in the crystal $\alpha(m_{x,y},p_{x,y})$, $\sigma(m_z,p_{x,y})$, and $\pi(m_{x,y},p_z)$ polarizations. [d] The g values are derived from pure $t_{2e}{}^2t_{2e}{}^2$ functions. g is the effective spin-only value in the limit of zero spin−orbit coupling, and k_e is the one-electron orbital reduction factor for t_{2g} orbitals.

We assume that the effects of spin−orbit coupling on the spin g value are not large, and in our empirical analysis of the Zeeman spectra we provisionally use $g \sim 2$. The orbital g value for the $^3E''$ state is defined as $\langle E_\pm{}''|L_z|E_\pm{}''\rangle = K(^3E'')$. The magnitude of $K(^{2S+1}\Gamma)$ depends on the detailed composition of the $^3E''$ state. In Table 2 we have assumed that the wave functions can be approximated by the pair functions derived from the $t_{2e}{}^2t_{2e}{}^2$ configuration so that

$$K((^3A_2{}^1E)\ ^3E'',^3E') = 2k_e$$

$$K((^1E^1E)\ ^1E') = -4k_e$$

$$K((^1E^1A_1)\ ^1E'',^1E'') = 2k_e \tag{12}$$

where in the limit of a pure $t_{2e}{}^2t_{2e}{}^2$ configuration the effective parameter k_e reduces to the one-electron orbital reduction parameter $k = (-)i\langle t_{2x}|l_z|t_{2y}\rangle$. In general, k_e will differ for different multiplets.

The calculations of k_e based on the $(t_{2e}e)^2(t_{2e}e)^2$ model are summarized in Figure 5. Note that the change in k_e is nearly all due to the variation in $h(x,e_x)$ which is related to J_π through expressions 9 and 10. This is confirmed by calculations where J_π is held constant and $h(x,e_x)$ is treated as an independent parameter. The new source of the orbital moments is the off-diagonal matrix element $\langle t_{2x}|l_z|e_y\rangle = i\sqrt{2}k'$.

Figure 5 shows several qualitative features which find support in the following empirical analysis of the optical spectra. First, the k_e parameters for both $^3E''$ and $^1E''$ states are significantly reduced as $h(x,e_x)$ and hence J_π increase. This is a consequence of the increase in e_g−t_{2g} mixing that is also responsible for an increase in the "trigonal" splitting of the $^3E''$ and $^3E'$ states. The e_g admixtures in the $^3E'$ and $^1E'$ states evidently have opposite phases, and in these cases k_e increases with $h(x,e_x)$. Thus for the $^3E'$ state $2k_e$ approaches the effective spin-only values. The previous difficulty[10] in detecting the second excited

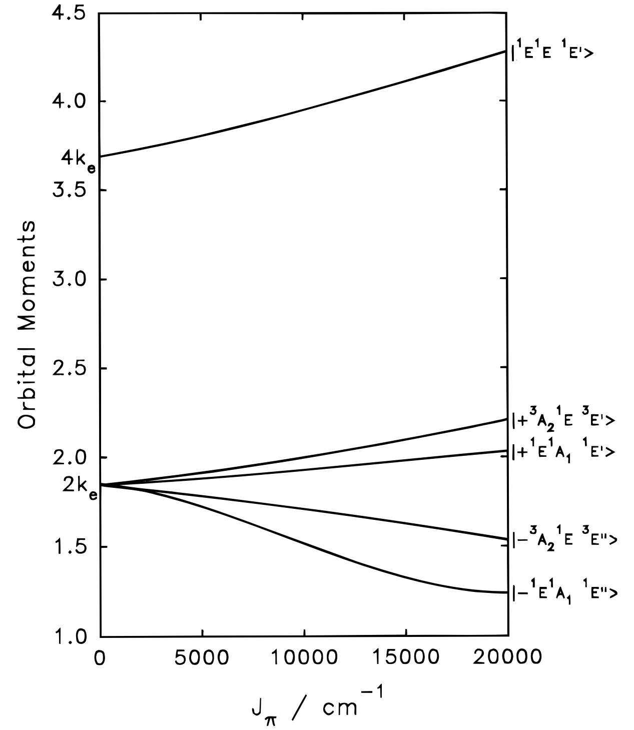

Figure 5. Dependence of the orbital reduction parameters k_e (derived from the $(t_{2e}e)^2(t_{2e}e)^2$ model) on J_π. The input parameters were $k = 1$, $B = 400$, $C = 1600$, $Dq = 2000$, $h(e_x,e_x) = 2000$, and $U = 20\,000$ cm^{-1}. The change in k_e is nearly all due to the change in $h(x,e_x)$ and follows J_π because $J_\pi = 36h(x,x)^2/U$ and we have assumed $h(x,e_x) = -\sqrt{2}h(x,x)$ (eqs 9 and 10).

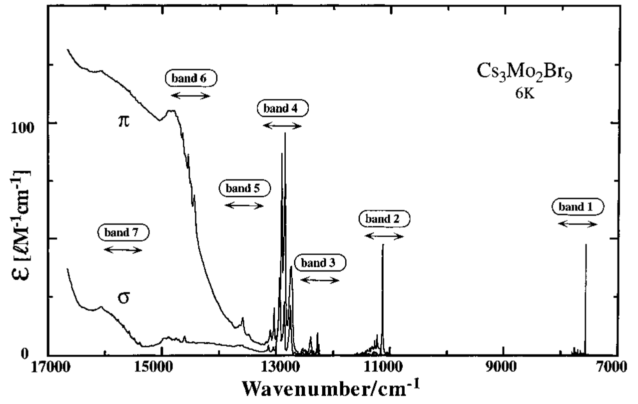

Figure 6. Single-crystal polarized absorption spectrum of Cs$_3$Mo$_2$Br$_9$ at 6 K.

state ^{3}E′ may now be resolved. Furthermore, a very large orbital g value is predicted for the (^{1}E^{1}E)^{1}E′ state, even when the reduction in k_e caused by covalency is taken into account.

Results and Discussion

General Spectral Features. The polarized spectra of Cs$_3$Mo$_2$Br$_9$ and Cs$_3$Mo$_2$Cl$_9$ are shown in Figures 6 and 7, respectively. The two spectra are very similar in band positions, relative intensities and polarizations. Most bands are predominantly π polarized except for the absorption near 7500 cm^{-1}. The bands of the bromide are shifted by 300−800 cm^{-1} to lower energy compared to those of the chloride complex.

A new and mainly π-polarized absorption, band 5, was observed for the bromide. Closer examination of the absorption near 13 700 cm^{-1} reveals that band 5 also occurs in the chloride spectrum, but in this case it overlaps with band 4 and gives the impression of stronger vibronic activity and longer progressions for band 4 in the spectrum of Cs$_3$Mo$_2$Cl$_9$.[10,11]

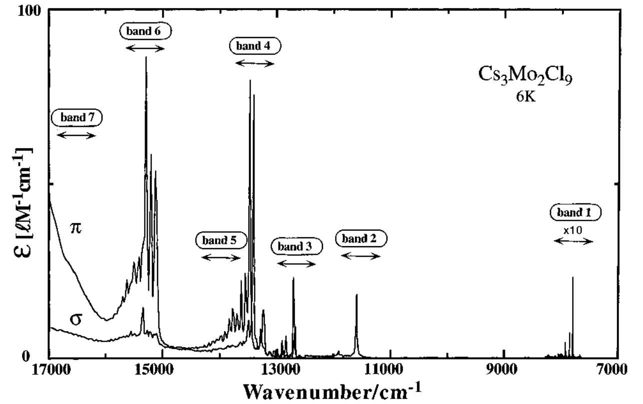

Figure 7. Single-crystal polarized absorption spectrum of Cs$_3$Mo$_2$Cl$_9$ at 6 K.

Table 3. Vibrational Energies of Cs$_3$Mo$_2$Br$_9$[a]

	vibrational modes/cm^{-1}				
D_{3h} symmetry	ν_1	ν_2	ν_3	ν_4	ν_5
A$_1$′		195	138	97	
A$_2$″	221	165	70	35	
E′	253	170	113	70	53
E″	232	141	115		48

[a] Data taken from both vibrational studies[20] and electronic spectra (*vide infra*).

An important result is the observation of band 7, which exhibits a rich vibronic structure, strong MCD, and large g values. A careful re-examination of this region revealed that band 7 also exists for the chloride.

Finally, the activities of the vibrations, particularly the A$_1$′ modes, of the Mo$_2$X$_9$ pair, vary between the different multiplets and, even for a given multiplet, they vary remarkably between the chloride and bromide. To aid in the discussion to follow, Table 3 gives the vibrational energies for Cs$_3$Mo$_2$Br$_9$ that were obtained from both Raman and infrared studies[20] and from the vibronic fine structure of the electronic spectrum (*vide infra*).

Band 1 (7400−7900 cm^{-1}). This spectral region exhibits complicated vibronic fine structure, and only the main features will be discussed. From Figure 4 and Table 2, the lowest excited multiplet is ^{3}E″(^{3}A$_2$^{1}E), which consists of A$_1$′ + A$_2$′ + E′ + E″ spin−orbit levels, and only the transition to E′ is electric dipole allowed in σ polarization. For Cs$_3$Mo$_2$Cl$_9$, the absorption near 8000 cm^{-1} (band 1) was shown to be due entirely to transitions to the ^{3}E″ multiplet.[10,13] The absorption near 7500 cm^{-1} in Cs$_3$Mo$_2$Br$_9$, shown in Figure 6, is similarly assigned. The σ- and π-polarized spectra of Cs$_3$Mo$_2$Br$_9$ between 7400 and 7900 cm^{-1} at 6 K are shown in Figure 8. The Zeeman spectra at 5 T are expanded in Figure 9 to highlight weaker features. The axial absorption and corresponding MCD spectra at 5 T are shown in Figure 10.

The σ polarization is dominated by the strong origin at 7574 cm^{-1}. Two weaker lines occur at 7661 and 7769 cm^{-1}, but the latter line has an identical Zeeman splitting and MCD sign as the origin and is therefore a totally symmetric vibrational sideband involving the ν_2(A$_1$′) mode of ~195 cm^{-1}. For Cs$_3$Mo$_2$Cl$_9$, however, the ν_4(A$_1$′) vibration with an energy of 127 cm^{-1} is active in the ^{3}E″(E′) state while ν_2(A$_1$′) is inactive.

The Zeeman splitting of the σ origin gives $g_z = 3.2$, indicating both spin and orbital contributions to the magnetic moment. On the basis of its strong intensity and negative MCD sign, it is assigned to the ^{3}E″(E′) spin−orbit level. From Table 2, a Zeeman splitting of $\mp(g + 2k_e)$ is predicted, where g is the

---

(20) Smith, P. W.; Stranger, R. *Aust. J. Chem.* **1986**, *39*, 1269.

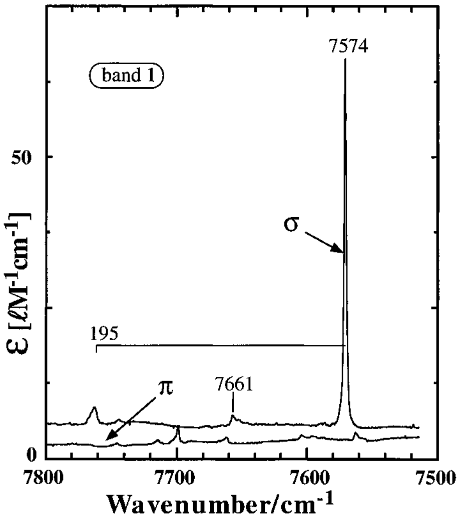

Figure 8. Polarized absorption spectrum of band 1 for $Cs_3Mo_2Br_9$ at 6 K.

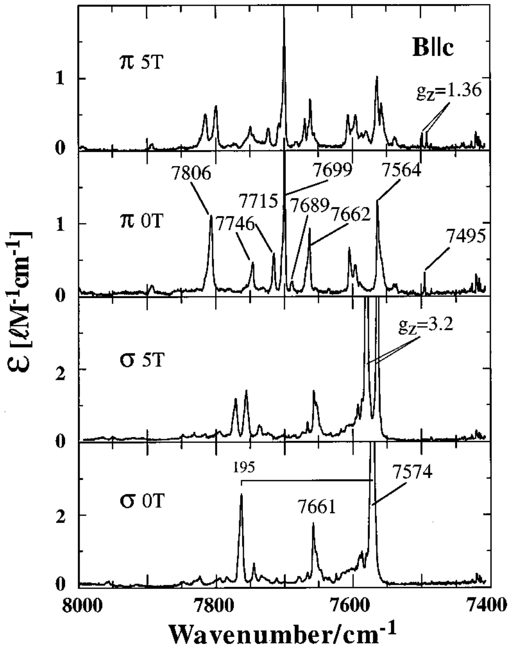

Figure 9. Polarized absorption and transverse Zeeman (light⊥*c*, *B*||*c*) spectra of band 1 for $Cs_3Mo_2Br_9$ at 1.6 K.

effective spin-only value and k_e is the one-electron orbital reduction factor. If we assume $g \sim 2$, then $k_e \sim 0.6$ is obtained for the $^3E''$ multiplet, compared to $k_e \sim 0.3$ found for the same origin in $Cs_3Mo_2Cl_9$.[10] As shown previously[12] and as shown under Theory, the k_e parameter for the $^3E''$ multiplet is strongly dependent on the magnitude of $h(x,e_x)$ and through eq 10 it depends also on J_π. The higher value of k_e for $Cs_3Mo_2Br_9$ is therefore attributed to a decrease in J_π relative to that for the chloride complex and is consistent with the 0.17 Å increase in the metal−metal distance in the bromide complex.

The σ line at 7661 cm^{-1} is not associated with the main origin at 7574 cm^{-1}, as the Zeeman splitting is too small to be resolved. Both the Zeeman and the MCD spectra of this line are complicated and indicate the overlap of two or more vibronic origins. The following analysis of the π spectra shows that both the E″ and $A_1' + A_2'$ electronic origins lie below the strong σ origin. Consequently, the 7661 cm^{-1} σ line must be assigned to a vibronic origin associated with either the E″ or $A_1' + A_2'$ spin−orbit levels.

The π polarization of band 1 is substantially weaker, and most lines are vibronically induced since transitions to the $^3E''$ multiplet are electric dipole forbidden in π polarization. The π line at 7495 cm^{-1} is very weak and sharp (fwhh of 0.5 cm^{-1}). This line also occurs in the axial absorption spectrum shown in Figure 10 but not in σ polarization and therefore must be assigned to the magnetic-dipole-allowed $^3E''(E'')$ spin−orbit level. The symmetric Zeeman splitting (Figure 9) and positive MCD (Figure 10) are consistent with this assignment and give $g_z = 1.36$. Since the predicted Zeeman splitting for the $^3E''(E'')$ origin is $\pm 2k_e$, we obtain $k_e \sim 0.7$, in good agreement with $k_e \sim 0.6$ derived for the $^3E''(E')$ origin.

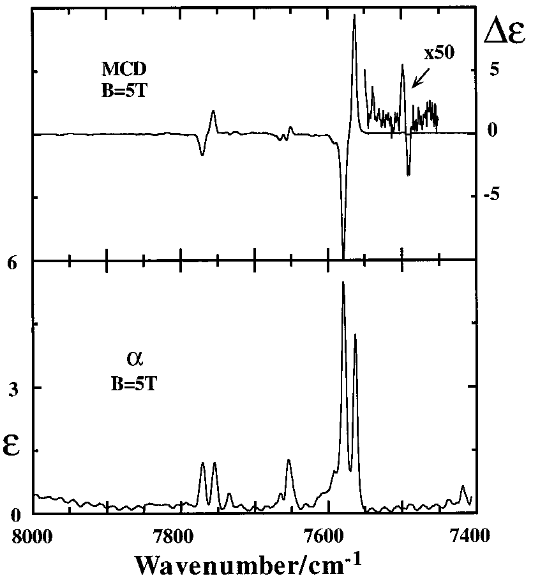

Figure 10. Axial absorption and MCD spectra of band 1 for $Cs_3Mo_2Br_9$ at 1.6 K.

In Figure 9, the π lines at 7689, 7715, and 7806 cm^{-1} have the same large Zeeman splitting, $g_z \sim 3.2$, as the σ origin. They must therefore be vibronics based on the $^3E''(E')$ level and assigned as ν_3, ν_2, and ν_1 E″ vibrations with energies of 115, 141, and 232 cm^{-1}, respectively. The same coupling pattern was observed for the $^3E''(E')$ level in the chloride spectrum.

The π lines at 7564, 7662, 7699, and 7746 cm^{-1} all exhibit asymmetric Zeeman splittings, indicating that the vibronics are associated with the electric-dipole-forbidden $^3E''(A_1' + A_2')$ spin−orbit levels. From Table 2, the $A_1' + A_2'$ spin−orbit levels have an off-diagonal Zeeman term of $\mp(g - 2k_e)$ which gives rise to an asymmetric Zeeman splitting because the A_1' and A_2' levels have a small zero-field splitting. To gain electric dipole intensity in π polarization, the $A_1' + A_2'$ levels must couple with either A_1'' or A_2'' vibrational modes. The sign of the asymmetric splitting, whether the most intense Zeeman line lies to higher or lower energy, varies from line to line, indicating that both A_1'' and A_2'' vibrational modes are vibronically active.

The temperature dependence measurements shown in Figure 11 reveal a weak hot band at ~7435 cm^{-1} associated with the 7564 cm^{-1} cold vibronic origin. This places the $A_1' + A_2'$ spin−orbit levels at approximately 7500 cm^{-1}, very near the $^3E''(E'')$ electronic origin at 7495 cm^{-1}. The energy difference between the hot and cold bands indicates an inducing mode of approximately 65 cm^{-1} which corresponds closely to the $\nu_3(A_2'')$ vibration. The proximity of the E″ and $A_1' + A_2'$ spin−orbit levels may explain the complicated Zeeman structure observed for a number of σ and π vibronic origins to higher energy. For instance, the σ line at 7661 cm^{-1} may consist of two vibronics, E″ coupled with $\nu_2(A_2'')$ and $A_1' + A_2'$ coupled with $\nu_2(E')$.

Band 2 (11 100−11 600 cm^{-1}). According to Figure 4, there

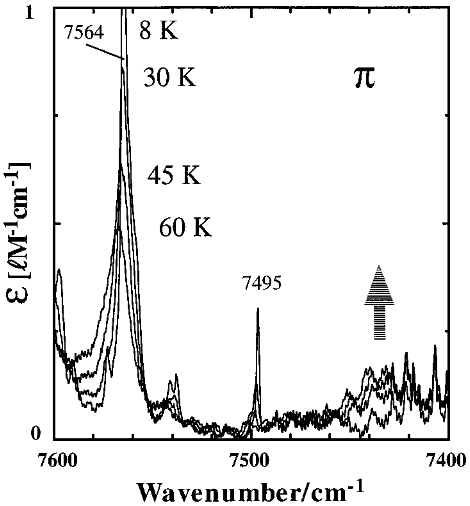

Figure 11. Temperature dependence of π polarization for band 1 in the spectrum of $Cs_3Mo_2Br_9$.

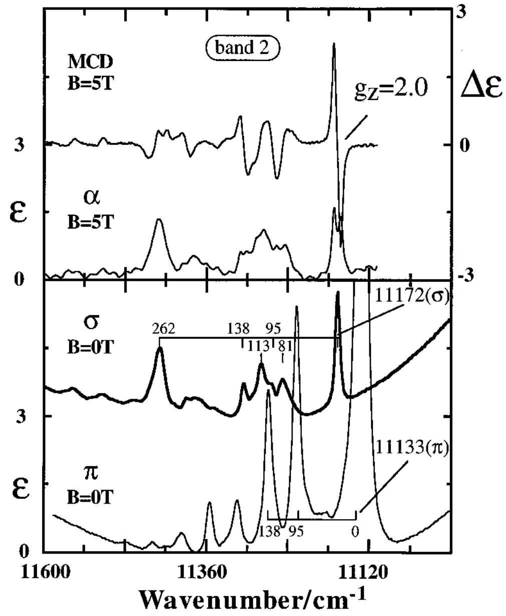

Figure 12. Polarized (σ,π) absorption and axial absorption and MCD spectra at 1.6 K of band 2 for $Cs_3Mo_2Br_9$.

are two possible assignments for band 2, the $^3A_1''(^3A_2{}^1A_1)$ and $^3E'(^3A_2{}^1E)$ multiplets. The analogous absorption for $Cs_3Mo_2Cl_9$ is seen at ~11 500 cm^{-1}. The σ- and π-polarized spectra and the axial absorption and MCD spectra at 1.6 K are shown in Figure 12. The line widths are much broader compared to those of band 1, and π spectra are much more intense than σ. The absorption band is dominated by the strong π origin at 11 133 cm^{-1}. Both the $^3A_1''(^3A_2{}^1A_1)$ and $^3E'(^3A_2{}^1E)$ multiplets consist of A_2'' and E' spin−orbit levels which are electric dipole allowed in π and σ polarizations, respectively. The π origin at 11 133 cm^{-1} is therefore assigned to the A_2'' spin−orbit level. Progressions in the $\nu_3(A_1')$ and $\nu_4(A_1')$ totally symmetric modes account for all the π lines observed to higher energy.

The σ absorption displays a more extensive and congested vibronic fine structure. The sharpest feature at 11 172 cm^{-1} is assigned to the E' spin−orbit origin. From Table 2, a positive MCD signal is expected for either the $^3A_1''$ or $^3E'$ assignment. The σ lines displaced by 95 and 138 cm^{-1} exhibit positive MCD and are therefore vibronic sidebands involving the $\nu_4(A_1')$ and $\nu_3(A_1')$ vibrational modes, respectively. The σ lines displaced by 80 and 112 cm^{-1} have negative MCD and must be assigned to vibronics involving $\nu_4(E')$ and $\nu_3(E')$ vibrations, respectively.

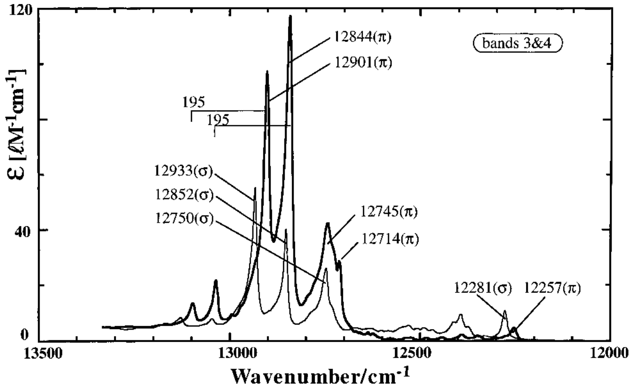

Figure 13. Polarized absorption spectrum of bands 3 and 4 for $Cs_3Mo_2Br_9$ at 6 K.

The σ line displaced by 262 cm^{-1} exhibits an overall negative MCD which is consistent with coupling of the E' origin with an $\nu_1(E')$ vibration of ~260 cm^{-1}. However, the MCD fine structure and large bandwidth indicate other contributions to this absorption.

From Table 2, the Zeeman splitting for the E' origin is $\pm g$ if assigned to the $^3A_1''$ multiplet and $\pm 2k_e$ if assigned to the $^3E'$ multiplet. From the $(\Delta A/A)_{max}$ value in the MCD spectrum, we obtain $g_z \sim 2.0$ in agreement with the spin-only g value predicted for the $^3A_1''(E')$ spin−orbit level. However, the g value of 2 is not inconsistent with the alternative assignment, as calculations[12] show that k_e is close to 1 for the $^3E'$ multiplet. Although covalency will reduce k_e, the increase in k_e from e_g−t_{2g} admixing may be greater than indicated in Figure 5 owing to the uncertainty in the value of $h(x,e_x)$ and in the accuracy of eq 10. Therefore, we are unable to distinguish between these two assignments on the basis of the magneto−optical data. However, the large splittings of the $^1E^1E$ double excitations, which are caused by moderately large J_π, are well accounted for by the theory, and it seems unlikely that the corresponding $^3A_2{}^1E$ single excitations would depart significantly from the theoretical predictions. Consequently, the assignment of band 2 to the $^3E'(^3A_2{}^1E)$ multiplet appears to be more reasonable. Transitions to the $^3A_1''$ multiplet are then assumed to be weak. They may overlap with band 2 and contribute to the absorption near 11 400 cm^{-1}. In the earlier work, band 2 was assigned to the $^3A_1''$ multiplet, since the possibility that J_π could be greater than 5000 cm^{-1} was not taken seriously and the k_e values for the $^3E''$ and $^3E'$ states were assumed to be identical.

Bands 3 and 4 (12 200−13 300 cm^{-1}). The σ and π polarizations of bands 3 and 4 are shown in Figure 13. This absorption region has no MCD, and therefore the excited states have no spin or orbital angular momentum. The spectra closely resemble those of the chloride complex and have been assigned as transitions to the doubly-excited $^1E^1E$ levels. As seen from Figure 4, this multiplet splits into $^1A_1''$, $^1A_1'$, and $^1E'$, and the $^1E'$ state is predicted to lie more than 2000 cm^{-1} above the $^1A_1''$ state. For the chloride complex, the separation between $^1A_1''$ and $^1A_1'$ origins was estimated to be ~700 cm^{-1}. Consequently, the entire absorption in the region 12 200−13 300 cm^{-1} for $Cs_3Mo_2Br_9$ is attributed to transitions to the $^1A_1''$ and $^1A_1'$ states, and this assignment is consistent with the absence of MCD for this band.

Below 12 700 cm^{-1}, the σ spectrum is slightly more intense than π for both bromide and chloride complexes. The polarized spectra consist of a σ false origin at 12 281 cm^{-1} and a π false origin at 12 257 cm^{-1}, from which all the higher lying fine structure up to 12 600 cm^{-1} can be accounted for by progressions in ν_4, ν_3, and ν_2 A_1' modes, as shown in Figure

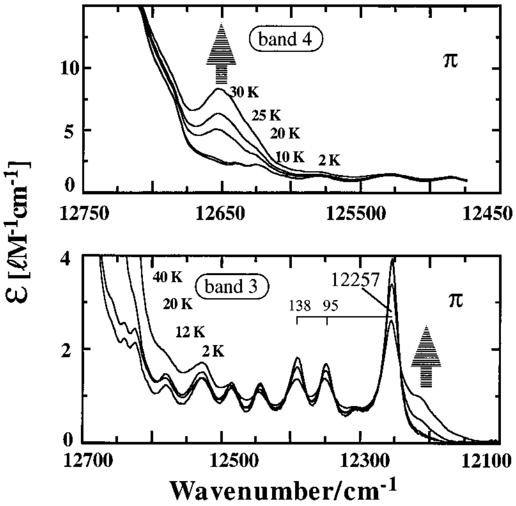

Figure 14. Temperature dependence of π polarization of bands 3 and 4 for $Cs_3Mo_2Br_9$.

14. Both the σ and π origins must be vibronic, as the ${}^1A_1' \rightarrow {}^1A_1''$ transition is both electric and magnetic dipole forbidden. From the temperature dependence of the π spectrum shown in Figure 14, a hot band is observed at ~12 210 cm^{-1}. If this hot band is associated with the false origin at 12 257 cm^{-1}, then the ${}^1A_1''$ electronic origin is predicted to lie at ~12 233 cm^{-1} and the inducing vibration has A_2' symmetry with an energy of ~24 cm^{-1}. The very low energy of this inducing mode is consistent with the sharp rise in hot band intensity seen in Figure 14. The σ false origin at 12 281 cm^{-1} must therefore involve the coupling of an E'' vibration with an energy of ~48 cm^{-1}, corresponding to $\nu_5(E'')$. The corresponding chloride spectrum also exhibits dramatic temperature dependence associated with coupling to low-energy-inducing modes.[18]

Above 12 700 cm^{-1}, both the σ and π spectra exhibit three main origins from which the remaining fine structure is due to progressions in the $\nu_2(A_1')$ vibration with an energy of ~195 cm^{-1}. In σ polarization, the three lines are located at 12 750, 12 852 and 12 933 cm^{-1}. These origins are all vibronically induced, arising from the coupling of the forbidden ${}^1A_1'$ electronic state with ν_4, ν_2, and ν_1 E' vibrations, respectively. The lowest energy origin also exhibits both higher and lower energy shoulders which may be assigned to weaker vibronics arising from the coupling of ν_3 and ν_5 E' vibrations, respectively. In π polarization, the three main vibronics occur at 12 745, 12 844, and 12 901 cm^{-1}, corresponding to coupling of the ${}^1A_1'$ electronic origin with ν_3, ν_2, and ν_1 A_2'' vibrations, respectively. The 12 745 cm^{-1} line also exhibits lower energy structure. The component at 12 714 cm^{-1} is sharp and corresponds to the coupling of the ${}^1A_1'$ origin with the $\nu_4(A_2'')$ mode of ~40 cm^{-1}. From the σ and π vibronics, the forbidden ${}^1A_1'$ state is estimated to lie near 12 680 cm^{-1}. This is supported by the observation of extremely temperature-dependent hot bands in π polarization (see Figure 14) at ~12 650 cm^{-1}, presumably associated with the cold vibronic at 12 714 cm^{-1}.

Band 5 (13 400–13 900 cm^{-1}). The σ and π spectra of band 5 are shown in Figure 15. A similar absorption occurs in $Cs_3Mo_2Cl_9$ near 13 750 cm^{-1} (Figure 7), where it overlaps with band 4 and makes the vibrational progressions appear to be more extensive than for the bromide complex. For the bromide complex, the relative intensities and separations of the π lines at 13 482, 13 589, and 13 645 cm^{-1} and the σ lines at 13 595 and 13 676 cm^{-1} are very similar to the vibronic structure associated with the $({}^1E{}^1E){}^1A_1'$ absorption between 12 600 and 13 200 cm^{-1}. It therefore seems likely that the vibronic structure of band 5 is also associated with an A_1' spin–orbit level. As seen from Figure 4, for moderate values of J_π, the ${}^3A_2'$ multiplet, derived from the ${}^3A_2{}^1A_1$ state, is predicted to lie between $({}^1E{}^1E){}^1A_1'$ and $({}^1E{}^1E){}^1E'$. The ${}^3A_2'$ multiplet consists of A_1' and E'' spin–orbit levels, and band 5 is tentatively assigned to the A_1' spin–orbit component. No MCD is observed in this region. The magnetic-dipole-allowed ${}^3A_2'(E'')$ level is expected to be very weak and broad and is unlikely to be detected. However, we have to assume that the vibronic coupling to the ${}^3A_2'(E'')$ level is also very weak.

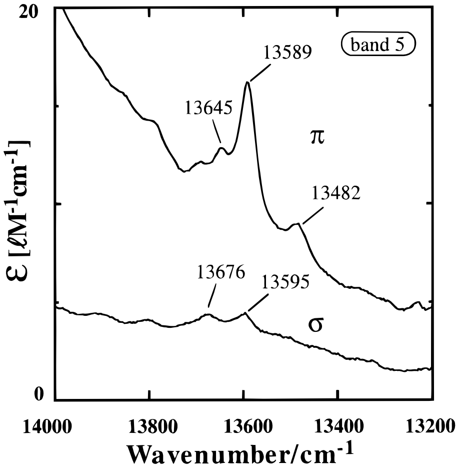

Figure 15. Polarized absorption spectrum of band 5 for $Cs_3Mo_2Br_9$ at 6 K.

Band 6 (14 400–15 200 cm^{-1}). The optical data for band 6 are given in Figure 16. The bandwidths and intensity are similar to those of bands 3 and 4, and the MCD indicates spin or orbital degeneracy in the excited state. From Figure 4, only two assignments of the excited state are possible, $({}^1E{}^1E){}^1E'$ and $({}^1E{}^1A_1){}^1E''$.

Band 6 for the chloride complex has been assigned[10] to the ${}^1E'$ state on the basis of the g values. From the MCD of the σ line at 15 333 cm^{-1} (Figure 2 in ref 10), g_z was estimated to be 0.6–1.0. The ${}^1E'$ assignment implied that $4k_e \sim 0.6-1.0$ and was in good agreement with the value $2k_e \sim 0.5$ obtained from the Zeeman spectra of band 1.

The former analysis is not valid because we now know that the Mo–Mo π bonding tends to increase the g_z value of $({}^1E{}^1E){}^1E'$ state and reduces k_e for the $({}^3A_2{}^1E){}^3E''$ and $({}^1E{}^1A_1){}^1E''$ states (Figure 5). The MCD of the prominent σ line at 14 608 cm^{-1} for the bromide complex (Figure 16) gives $g_z \sim 1.8$. Since even larger g values are observed for band 7 (next section), we must assign band 6 for both the bromide and the chloride to the ${}^1E''$ multiplet. The g_z value for the bromide implies that $2k_e \sim 1.8$ for the ${}^1E''$ level and is significantly greater than that for the chloride, a fact consistent with the stronger Mo–Mo π bonding in the chloride complex. The same difference in the k_e values between the bromide and the chloride complexes is observed for the $({}^3A_2{}^1E){}^3E''$ state (band 1).

Since transitions to the ${}^1E''$ state are electric dipole forbidden, the prominent σ line at 14 608 cm^{-1} must be a vibronic. Most of the higher lying structure has MCD with the same sign as the σ false origin and can be assigned to progressions in ν_4, ν_3, and ν_2 A_1' vibrations.

The strong σ line at 14 608 cm^{-1} and the weaker σ lines at 14 543 and 14 455 cm^{-1} all have the same MCD sign and must be assigned to vibronics derived from the coupling of the ${}^1E''$ origin with either A_1'' or A_2'' vibrations. The energy separation between these false origins is consistent with coupling to ν_3, ν_2, and ν_1 A_2'' vibrations, and the ${}^1E''$ origin is estimated to lie at 14 375 cm^{-1}.

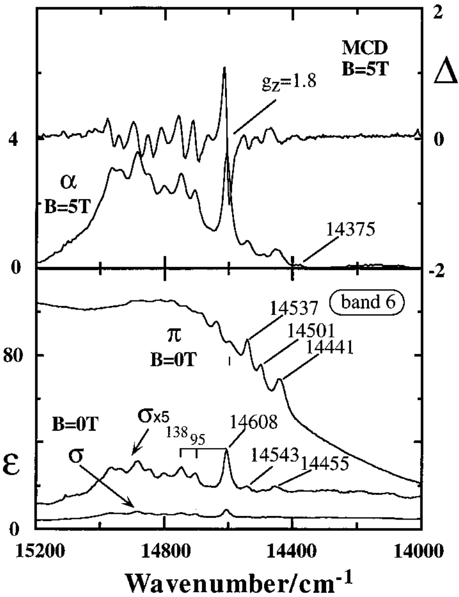

Figure 16. Polarized absorption (α,σ,π) and MCD spectra of band 6 for $Cs_3Mo_2Br_9$ at 1.6 K.

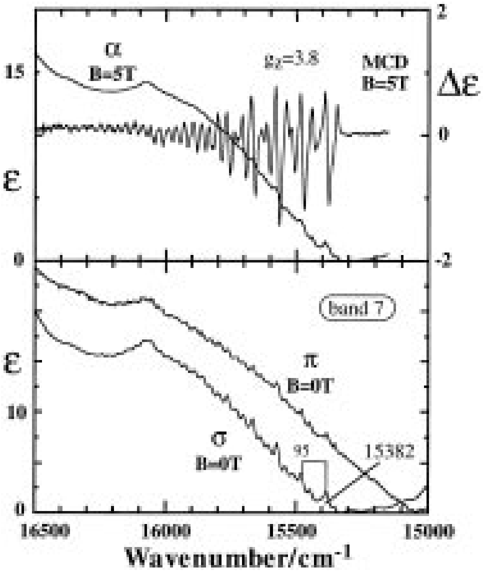

Figure 17. Polarized absorption (α,σ,π) and MCD spectra of band 7 for $Cs_3Mo_2Br_9$ at 1.6 K.

The true $^1E''$ origin is magnetic dipole allowed in axial polarization, and indeed a very weak line with positive MCD is observed in the axial spectrum at ~ 14 375 cm^{-1}. From this origin, the prominent π lines at 14 441, 14 501, and 14 537 cm^{-1} can be assigned to vibronics formed by coupling to ν_5, ν_3, and ν_2 vibrations of E′ symmetry.

Band 7 (15 000−15 600 cm^{-1}). The optical data for band 7 are given in Figure 17. The rich vibronic structure is mainly due to progressions in the $\nu_4(A_1')$ vibration with energy 95 cm^{-1} and based on three false origins at 15 354, 15 382, and 15 402 cm^{-1}. The analysis of the line shape of the MCD yields $g_z \sim 3.8$. The large value of g_z is also apparent in the α spectrum at 5 T where the Zeeman splittings of the false origins are partially resolved.

There is only one low-lying state that can have such a high g_z value, and from Table 2 the assignment $(^1E^1E)^1E'$ is unambiguous. This is also consistent with the theoretical model which indicates that the g value of the $(^1E^1E)^1E'$ state increases with increase in Mo−Mo π bonding (Figure 5).

The lines at 15 354 and 15 402 cm^{-1} have negative MCD while the more intense line at 15 382 cm^{-1} has positive MCD. The latter must involve the coupling of the $^1E'$ state with an E′ vibration, since the true origin must have an MCD A term of negative sign ($g_z \sim -3.8$). The true origin may lie at or below 15 106 cm^{-1}. A very weak and sharp line with $|g_z| \sim 3.9$ is observed at 15 106 cm^{-1} (Figure 16), but the MCD is poorly resolved and the sign of the A term is uncertain.

Exchange-Coupled-Pair Calculations. The calculated energies in Figure 4 give an approximate fit to the observed multiplets for $Cs_3Mo_2Cl_9$ with $J_\pi \sim 16\,000$ cm^{-1} and a slightly smaller value of J_π for $Cs_3Mo_2Br_9$. This result corresponds to the transfer integral $h(x,x) \approx -3000$ cm^{-1} if U (eq 2) is given the value 20 000 cm^{-1}. The Xα−SW calculations[9] give $h(x,x) = -2000\ (-1100)$ cm^{-1} for the chloride (bromide) complexes, respectively, and therefore suggest significantly smaller values for J_π. In fact they imply that $J_\pi(\mathrm{Cl})/J_\pi(\mathrm{Br}) \approx 4$, provided the t_{2z} orbitals are fully decoupled in both cases. The observed orbital g values for the first excited state ($^3E''$) do indicate a significantly smaller J_π for the bromide complex, but it appears that Figures 4 and 5 cannot be used quantitatively.

It seems that the J_π values in our calculations are almost a factor of 2 larger than expected from the Xα−SW calculations. Whether this is a consequence of the neglect of the $J_{\sigma\pi}$ parameter (incomplete decoupling of the t_{2z} orbitals) or errors in eq 10 or even the neglect of spin−orbit coupling we do not know. It is worth emphazing that the transfer energy U is a critical parameter in the pair calculations. It is defined on the basis of the differences between one-center and two-center repulsion integrals, $U = \langle \alpha\alpha|\alpha\alpha\rangle - \langle \alpha\beta|\alpha\beta\rangle$. The U parameter appears to have remarkably small values in dimers with strong M−M bonding,[17] so that the accuracy of the second-order expressions such as eqs 2 and 7 may be questioned. For example, U has been assigned[17] the values 10 000 cm^{-1} for $[Re_2Cl_4(PMe_2Ph)_4]^{1+/2+}$ up to 16 800 cm^{-1} for $[Mo_2(SO_4)_4]^{3-/4-}$.

Bonding in $Cs_3Mo_2X_9$ Complexes. The parameter that is directly related to the net Mo−Mo bonding is the transfer integral $h(\alpha,\beta)$. The SCF−Xα−SW calculations[9] gave $h(x,x) = -2000$ cm^{-1} for the chloride, a moderately large value for the bonding between the strongly misaligned t_{2e} orbitals. If we ignore the very small δ Mo−Mo bonding, the departure of the t_{2e} orbitals from the optimum alignment for Mo−Mo π bonding is so large that it seems appropriate in these cases to introduce fractional bond orders. Thus the bond order for $Cs_3Mo_2Cl_9$ is $1\sigma + {}^1/_3\pi + {}^1/_3\pi$, where π represents a standard Mo−Mo π bond.

However, the molecular orbital energy, $2h(x,x)$, associated with the ${}^1/_3\pi$ bonds is particularly sensitive to changes in the direct Mo−Mo bonding because it represents a balance between the negative contribution $h(x,x)_{MM}$ arising from direct Mo−Mo π bonding and a positive contribution from Mo−X(bridge) π bonding. If we apply the angular overlap model[19] to the Mo_2X_9 dimer and define the halide p orbitals to be p_y (tangential to the equilateral triangle of the bridging halides) and p_x (radially directed toward the center of the triangle), then for the case where the bridging angle Mo−X−Mo is 70.5° (corresponding to two fused octahedra) one can show that

$$h(x,x) = h(x,x)_{MM} + {}^3/_2 e_{\pi y} + {}^1/_6 e_{\pi x} - {}^1/_3 e_{\pi z}$$

Thus the donor bridging orbitals, principally the tangential p_y orbitals, give a significant π perturbation energy which tends to cancel the direct Mo−Mo π bonding. This cancellation is almost complete[9] for $Cs_3Mo_2I_9$ so that in this case the "${}^1/_3\pi$ bond" is so weak that there is no net π bonding. If the terminal halides are replaced by more electron-withdrawing groups, then $h(x,x)$ may reverse sign and the small π bonding will be entirely due to metal−bridging ligand π bonding or superexchange.

IC951581+